

Correlation Debiasing for Unbiased Scene Graph Generation in Videos

Anant Khandelwal
Glance AI
Bangalore, India

anant.iitd.2085@gmail.com

Abstract

*Dynamic scene graph generation (SGG) from videos requires not only comprehensive understanding of objects across the scenes that are prone to temporal fluctuations but also a model the temporal motions and interactions with different objects. Moreover, the long-tailed distribution of visual relationships is the crucial bottleneck of most dynamic SGG methods, since most of them focus on capturing spatio-temporal context using complex architectures, which leads to the generation of biased scene graphs. To address these challenges, we propose FLOCODE: **Flow**-aware temporal consistency and **Correlation Debiasing** with uncertainty attenuation for unbiased dynamic scene graphs. FLOCODE employs feature warping using flow to detect temporally consistent objects across the frames. In addition, it uses correlation debiasing to learn the unbiased relation representation for long-tailed classes. Moreover, to attenuate the predictive uncertainties, it uses a mixture of sigmoidal cross-entropy loss and contrastive loss to incorporate label correlations to identify the commonly co-occurring relations and help debias the long-tailed ones. Extensive experimental evaluation shows a performance gain as high as 4.1% showing the superiority of generating more unbiased scene graphs.*

1. Introduction

Scene graph generation for videos (VidSGG) aims to represent the video in the form of a dynamic graph that is able to capture the temporal evolution of the relationships between pairs of objects. VidSGG has direct usage for various downstream applications like visual question answering [1, 44, 52], video captioning [53] and video retrieval [8, 40, 51] etc. VidSGG is considered more challenging compared to its image-based counterpart since the relations between identified object pairs are dynamic along the temporal dimension, making this a multi-label problem. In the current stage, VidSGG is relatively in its nascent stage as compared to SGG (scene graph generation) from static images [7, 22–24, 27, 30, 43, 57, 58, 58]. Several

works [6, 11, 17, 26, 28, 36, 46] have proposed to solve VidSGG mostly with spatio-temporal sequence processing with transformers [3, 4, 12, 18, 32, 42, 49]. Most of these methods simply focus on building complex models that can effectively aggregate the spatio-temporal information in a video, but they eventually lack the ability to address the data imbalance in the relation/predicate classes. Their performance is quite good in terms of the Recall@K metric, which is biased towards frequent classes. However, another metric mean-Recall@K is proposed [5, 43] to quantify the performance in the presence of low-frequent classes, since it gives the overall view of the SGG models rather than considering only high-frequent classes. Although, recent methods [31, 35] has proposed to deal with class imbalance using memory-based debiasing and uncertainty attenuation for classification. But their method of debiasing is based on learnable attention and transformer weights, which have a risk of getting biased towards high-frequent classes. One such case of this issue has been shown in Figure 2 during qualitative comparison with our method. Moreover, the uncertainty attenuation based on Gaussian Mixture Models (GMM) has several limitations, as discussed in [34, 38, 56]. To overcome these limitations of GMM based classification, some works have proposed the regularization with a mixture of standard deviations [19] and some proposed loss function that can incorporate label correlations [38]. Some more approaches [25, 54] also tried to address the biased relation predictions. Li et al. [25] proposed to weaken the false correlation between input data and the predicate labels. Xu et al. [54] considered biases in a meta-learning paradigm. These approaches mitigate the long-tail problem to some extent, but the performance is still not satisfactory. In this work, we not only focus on improving the unbiased predicate classification but also on improving object detection. We proposed to use the flow-warped features in the temporal dimension to compensate for the dynamic fluctuations in a video. In our analysis (in Table 4), it is shown that the major bottleneck in the existing dynamic SGG is the incorrect detection of objects across the video frames. Moreover, as compared to previous methods[31] which use mem-

ory correlation to debias the predicate embedding, it has the risk of biasing the attention weights towards highly frequent classes. In order to mitigate this, we propose to debias the predicate embeddings during the generation stage itself, since the correlation between the predicate embeddings and the entities is primarily driven by high-frequent relation classes, and hence we make this correlation unbiased so that the learned embeddings are themselves the debiased embeddings. Furthermore, the uncertainty attenuation in existing methods[31] does not take into account the label correlations. Hence, we proposed to use a mixture of logic networks (MLNs) that can distinguish between two different types of predictive uncertainty: aleatoric and epistemic uncertainty. In addition to the uncertainty-aware classification loss, we introduced supervised contrastive loss to take into account the label correlations. The objective of multi-label contrastive loss is to pull together predicate representations having more than one overlapping class while pushing apart negative samples that do not share any classes. Further, we regularize the uncertainty-aware training loss function with aleatoric and epistemic uncertainty to penalise the loss function explicitly, which can reduce the uncertainty, especially for low-frequent classes where the probability of incorrect prediction is high. Combining all this, we named our framework FLOCODE: **Flow**-aware temporal consistency and **Correlation Debiasing** with Uncertainty Attenuation for an unbiased dynamic SGG. The major contributions of this paper are: 1) FLOCODE models both (a) aleatoric and epistemic uncertainty associated with dynamic SGG and (b) label correlations to produce more unbiased scene graphs. 2) Utilising a novel correlation-guided debiased learning of predicate embeddings that avoids the bias in learnable weights of attention and transformer decoder. 3) Utilising flow-aware, temporally consistent object detection for accurate classification of nodes in scene graphs 4) FLOCODE achieves significant gains for mR@K[43] and R@K, highlighting its superiority in generating unbiased scene graphs.

2. Related Work

Image Scene Graph Generation: Image-based scene graph generation (ImgSGG) is the task of obtaining the structured graph summarization that involves objects as nodes and their relationships (formally called predicates) as edges in an image. There exists tremendous work on ImgSGG with comparison to a common benchmark, Visual Genome (VG) [22]. Some of these focused on evolving efficient ways of aggregating spatial context [24, 27, 30, 57, 58] while some of the latest works are based on addressing fundamental problems such as preventing biased scene graphs caused by long-tailed predicate distribution and noisy annotations in dataset.

Video Scene Graph Generation (VidSGG): With the successful exploration of spatial context within images, video researchers have started to explore the spatial context and

temporal correlation between objects detected across the frames. Similar to ImgSGG, long-tailed predicates and noisy annotations still exist in the VidSGG benchmark Action Genome [16]; further, it has the additional challenge of addressing the temporal fluctuations across the frames. Numerous approaches [28, 36, 46, 48, 59] have employed object-tracking mechanisms to tackle the temporal fluctuations among different frames. However, object-tracking models incur high computational costs and memory consumption; they also accumulate information from irrelevant frames, leading to suboptimal performance. STTran [6] proposes a strong baseline that adopts a spatial encoder and a temporal decoder to extract implicitly spatial-temporal contexts. Other works [26, 50] which are also based on extracting temporal correlations. Some ensure temporal continuity by extracting the entire co-occurrence pattern, while others propose pre-training paradigms to model the temporal correlations implicitly. A lot of works [3, 32, 42, 49] are based on the superior sequence processing ability of transformers for the spatio-temporal context of visual relations. However, despite their success, these are mostly providing gains for high-frequent classes and suffer from the problem of long-tail bias. Recent work TEMPURA[31] tries to address the long-tail problem using an uncertainty-guided loss function. We go beyond this and explore label correlation to further reduce prediction uncertainty.

3. Method

3.1. Preliminary

Problem Statement: Given a video $\mathcal{V} = \{I_1, I_2, I_3, \dots, I_T\}$, the goal of dynamic SGG is to generate scene graphs denoted as $\mathcal{G} = \{G_t\}_{t=1}^T$ of video V consisting of T frames. $G_t = \{V_t, E_t\}$ is the scene graph of frame I_t , where V_t is the set of nodes and E_t is the relation as edges between nodes in V_t . Nodes V_t connected to each other using predicate in E_t , forming multiple $\langle \text{subject-predicate-object} \rangle$ triplets. The set of object and predicate classes are referred to as $\mathcal{Y}_o = \{y_{o1}, y_{o2}, y_{o3}, \dots, y_{o_{c_o}}\}$ and $\mathcal{Y}_r = \{y_{r1}, y_{r2}, y_{r3}, \dots, y_{r_{c_r}}\}$ respectively.

Object Detection and Relation Representation: With the use of an off-the-shelf object detector (Faster-RCNN [37]), we obtain the set of objects $O_t = \{o_i^t\}_{i=1}^{N(t)}$, where $N(t)$ is the number of objects detected in frame I_t . Each object in a t^{th} frame is denoted as $o_i^t = \{b_i^t, v_i^t, c_{o_i}^t\}$ where $b_i^t \in \mathbb{R}^4$ being the bounding box, $v_i^t \in \mathbb{R}^{2048}$ the RoIAligned [14] proposal feature of o_i^t and $c_{o_i}^t$ is its predicted class. However, the object class $c_{o_i}^t$ fluctuates across the frames and is not coherent even for the same object. Existing works [46] address this by incorporating object tracking algorithms; opposed to this, our strategy compensates for these dynamic fluctuations using flow-warped features and ensures temporal coherence. Additionally, we extracted the base features $f_t, t \in [1, T]$ and ROIs from Faster R-CNN using ResNet-101 [13]. We warp these base features using

the temporal flow and compute the RoIAligned warped object features $v_i^{t \rightarrow t'}$ (t' represents the immediate previous frame that contains the i^{th} object) using the predicted ROIs.

3.2. Temporal Flow-Aware Object Detection

Object detectors trained on static images are prone to misclassifying the same object in different frames. Existing methods [6, 17, 26, 50] either use $c_{o_i}^t$ obtained from object detection in each frame or use object feature to classify objects. However, these methods do not compensate for temporal fluctuations in the videos. Inspired by FPGA[60], which uses flow-guided feature aggregation for object detection in videos, we propose to leverage flow-warped features and temporal processing for consistent object detection across frames. We introduce *Temporal Flow-Aware Object Detection (TFoD)*, which utilises transformer encoder [49] with masked self-attention (*TEnc*) to process the set of temporal object sequences $\mathcal{O}_{\mathcal{V}}$, which is constructed as follows:

$$\mathcal{O}_{\mathcal{V}} = \{\mathcal{O}_{t_1, k_1}^1, \mathcal{O}_{t_2, k_2}^2, \dots, \mathcal{O}_{\hat{C}_o, k_{\hat{C}_o}}^{\hat{C}_o}\}, \text{ where} \\ \mathcal{O}_{t_j, k_j}^j = \{v_i^t, v_i^{t+1}, \dots, v_i^k\} \quad (1)$$

Each entry of \mathcal{O}_{t_j, k_j}^j corresponds to an object of the same detected class c_{o_j} , here $1 \leq t_j, k_j \leq T$ and $\hat{C}_o \leq C_o$ denoting all the detected classes in a video \mathcal{V} . However, the detected class labels can be noisy since they are based only on frame-level predictions; hence, we use the flow-warped feature $v_i^{t \rightarrow t'}$ instead of v_i^t before feeding it to the transformer encoder. The flow-warped feature is computed as:

$$f_{t \rightarrow t'} = \mathcal{W}(f_t, \mathcal{F}(I_{t'}, I_t)) \quad (2)$$

where \mathcal{W} is a bilinear warping function [60, 61] applied on all the locations for each channel in the feature maps and flow field $\mathcal{F}(I_{t'}, I_t)$ is computed from the pre-trained FlowNet [9], where t' is the index of the immediate frame previous to the t^{th} frame having the same object as depicted in the object sequences $\mathcal{O}_{\mathcal{V}}$. Using $f_{t \rightarrow t'}$ and predicted ROIs, the warped RoIAligned feature is computed, and then the \mathcal{O}_{t_j, k_j}^j is denoted as:

$$\mathcal{O}_{t_j, k_j}^j = \{v_i^t, v_i^{t+1 \rightarrow t}, \dots, v_i^k\} \quad (3)$$

Each of \mathcal{O}_{t_j, k_j}^j is zero-padded to prepare functional input tensor. *Tenc* uses masked multi-head self-attention instead of multi-head self-attention in transformer encoder [49]. Mask is introduced to learn the temporal dependencies in a unidirectional manner so that the object at frame index t can only attend to objects in previous frames. Attending to future context can be noisy since it is more probable for unrelated objects, and hence it is noisy to attend to future

context. For any input \mathbf{X} , the single head masked attention \mathbb{A} is given as:

$$\mathbb{A}(\mathbf{Q}, \mathbf{K}, \mathbf{V}) = \text{softmax} \left(\frac{\text{mask}(\mathbf{Q}\mathbf{K}^T)}{\sqrt{D_K}} \right) \mathbf{V} \quad (4)$$

where D_K is the dimension of \mathbf{K} , and $\mathbf{Q}, \mathbf{K}, \mathbf{V}$ are the query, key, and value vectors, respectively. Here, $\mathbf{Q} = \mathbf{K} = \mathbf{V} = \mathbf{X}$, the multi-head attention is $\mathbb{M}(X) = \text{concat}(a_1, a_2, \dots, a_H)W_H$, where $a_i = \mathbb{A}(\mathbf{X}W_{Q_i}, \mathbf{X}W_{K_i}, \mathbf{X}W_{V_i})$ where $W_{Q_i}, W_{K_i}, W_{V_i}$ and W_H are the learnable weight matrices. The rest of the components, like residual connection, normalisation, and FFN (feed-forward network), remain the same as in the transformer encoder [49]. The output of n -layered *TEnc* is given as:

$$X_{out}^{(n)} = TEnc(X_{out}^{(n-1)}), X_{out}^{(0)} = \hat{O}_V \quad (5)$$

where $\hat{O}_V = \mathcal{O}_V + P_o^T$, where P_o^T are the fixed positional embeddings injecting the temporal position of objects. Inspired by the properties of neural collapse [33] we prefixed the classifier weights (forming Equiangular Tight Frame (ETF)) for each object class to induce the maximal separable classifier even under the class imbalance setting. The pre-fixed classifier weights \mathbf{W}_{ETF} are given as:

$$\mathbf{W}_{ETF} = \sqrt{\frac{C_o}{C_o - 1}} \mathbf{U} \left(\mathbf{I}_{C_o} - \frac{1}{C_o} \mathbf{1}_{C_o} \mathbf{1}_{C_o}^T \right) \quad (6)$$

where $\mathbf{W}_{ETF} = [\mathbf{w}_1, \mathbf{w}_2, \dots, \mathbf{w}_{C_o}] \in R^{d \times C_o}$, $\mathbf{U} \in R^{d \times C_o}$, allows a rotation and satisfies $\mathbf{U}^T \mathbf{U} = \mathbf{I}_{C_o}$, \mathbf{I}_{C_o} is the identity matrix, and $\mathbf{1}_{C_o}$ is an all-ones vector. The object classification loss is then given as:

$$\mathcal{L}_o(x_{o_i}, \mathbf{W}_{ETF}) = \frac{1}{2} \left(\mathbf{w}_{c_{o_i}}^T \hat{x}_{o_i} - 1 \right) \quad (7)$$

where $\hat{x}_{o_i} = x_{o_i} / \|x_{o_i}\|$ and $x_{o_i} \in X_{out}^{(n)}$ and $\mathbf{w}_{c_{o_i}}$ is the fixed prototype in \mathbf{W}_{ETF} for object class c_{o_i} and we have $\|\mathbf{w}_{c_{o_i}}\| = 1$. Finally, the converged features will be aligned with \mathbf{W}_{ETF} , and thus the ETF structure instructed by neural collapse is attained. This results in pulling the object features of the same class into a common prototype and pushing away the features of other classes. The theoretical advantage of the loss has been proved in [55].

3.3. Correlation-Aware Predicate Embedding

The relationship between objects is governed by three types of correlations: a) *spatial correlation between predicates* b) *temporal correlation between predicates* c) *predicate-object correlation across the video frames*. We propose to model these correlations using the Vanilla Transformer [49]. Since the relations between objects are highly imbalanced, the relation representation becomes biased towards popular ones, and hence, to produce unbiased relation embeddings, we

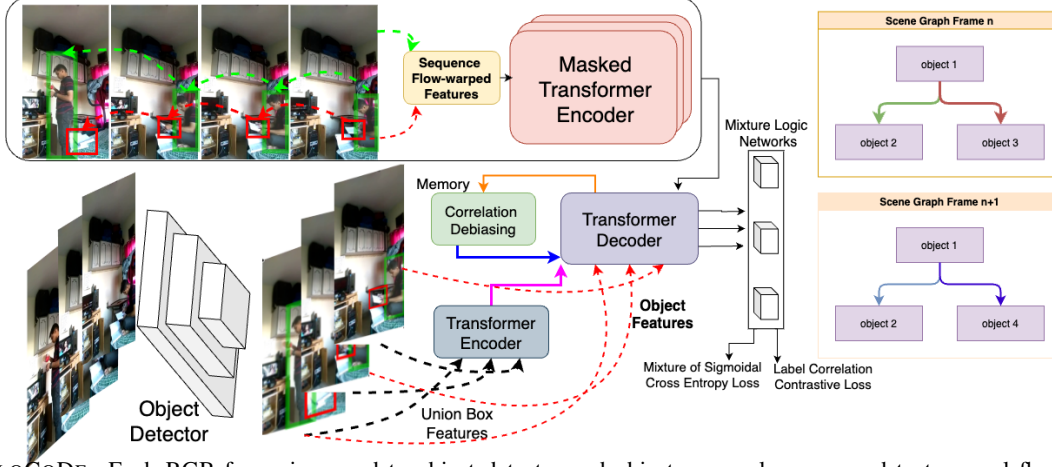


Figure 1. FLOCODE: Each RGB frame is passed to object detector and object proposals are passed to temporal flow-aware object classification and relation classification (correlation debiasing and MLN for uncertainty attenuation) to generate unbiased scene graphs

propose to update correlation matrices as a weighted average of the current correlation matrix and the previous matrix, where the weight is determined by the decay factor. For each object o_i of predicted class c_{o_i} obtained from object detection (Section 3.2), the input to the transformer encoder is the set of features describing the relation with each object o_j detected in all the frames where o_i is detected. The input is constructed as follows:

$$r_{i,j}^t = \text{concat}(\mathbf{x}_{c_{o_i}}, f_u(\mathbf{u}_{ij}^t + f_{box}(\mathbf{b}_i^t, \mathbf{b}_j^t)), f_I(t)) \quad (8)$$

where $\mathbf{x}_{c_{o_i}} \in X_{out}^{(n)}$ is the feature representation of object o_i belonging to class $c_{o_i} \in [1, C_o]$, $\mathbf{u}_{ij}^t \in \mathbb{R}^{256 \times 7 \times 7}$ is the feature map of the union box computed by RoIAlign [14]. f_u, f_I is the FFN based on non-linear projections, and f_{box} is the bounding box to feature map projection of [57]. Both are configured to produce d-dimensional relation features. f_I serve as positional embeddings denoting the frame index. The single encoder input consists of both spatial and temporal relation features between object o_i and all other objects. $\{o_1, o_2, \dots, o_j\}$, specifically it is constructed as $R_i = \{r_{i,1}^{t_1}, r_{i,2}^{t_2}, \dots, r_{i,j}^{t_j}\}$, where t_j are the frame indices where o_i and o_j are detected simultaneously. The transformer decoder leverages masked self-attention, and its input is a set of object representations. $\{\mathbf{x}_{c_{o_1}}, \mathbf{x}_{c_{o_2}}, \dots, \mathbf{x}_{c_{o_j}}\}$, corresponding to objects $\{o_1, o_2, \dots, o_j\}$, detected in all the frames where o_i is detected. The input to the transformer encoder contains all the predicate (relation) features across the frames, and hence, with multi-head self-attention, it models both spatial and temporal correlation between predicates. Similarly, the cross-attention between the encoder and decoder models the predicates-object correlation. The predicate embeddings at the output of the transformer decoder are denoted as $\hat{r}_{tem}^k = \hat{r}_{i,j}^t \forall k \in [1, N(t)], t \in [1, T]$. At transformer decoder, we use the sliding window of size 10 for predicate representation with relating objects.

3.4. Debaised Predicate Embedding

The relation embeddings at the output of the transformer decoder are biased by the fact that popular relations drive the learning of attention weights, causing the biased predicate embeddings. Hence, we update the cross-attention matrix with the previous matrix corresponding to each triplet $\{o_i, r_{i,j}, o_j\}$ obtained by attention between the transformer encoder and decoder across all the layers. Since the input to the transformer encoder is concatenated relation and object features, and hence using cross-attention with querying objects, we get the predicate-object correlations. Since some predicates are rare and hence more prone to getting biased, if we update their correlation using previously observed correlation, it will generate the debaised embeddings. Let's denote the stored correlation matrix between every object pair for all relations as \mathcal{M}_{e-1} at the end of the previous epoch $e-1$, and the attention matrix at the current ongoing epoch e is A_e . During training, we update the attention matrix (denoted as \hat{A}_e) using the decaying factor η as the training epoch progresses, given as:

$$\hat{A}_e(o_i, r_{i,j}, o_j) = \eta * A_e(o_i, r_{i,j}, o_j) + (1 - \eta) * \mathcal{M}_{e-1}(o_i, r_{i,j}, o_j) \quad (9)$$

where $\mathcal{M}_0 = A_0$ at the end of the zero epoch. We then use the attention value from \hat{A}_e in place of the attention value calculated from $QK^T \in A_e$. This avoids debiasing the attention weights to avoid biasing towards popular predicates. Once the debaised weights are learned during training, we expect that they will generate debaised embeddings during the inference phase. Hence, there is no modification of attention matrices during inference time.

3.5. Predicate Classification

Following previous works [31], we model the classifier framework to model the noisy annotations in the SGG data.

Specifically, we model the classification head as a mixture-of-experts model named mixture logit networks (MLN) and a noise pattern estimation method utilizing the outputs of the MLN. The number of mixtures is \mathcal{K} . Different from [31], we propose: 1) an uncertainty-aware mixture of attenuated loss 2) supervised contrastive learning, which incorporates label correlation to improve predicate classification. **Uncertainty-Aware Mixture of Attenuated loss:** For a sample embedding \mathbf{z}_i , the class-specific aleatoric (σ_a) and epistemic uncertainty (σ_e) are computed as:

$$\sigma_e^2 = \sum_{p=1}^{C_r} \sum_{k=1}^{\mathcal{K}} \pi_{i,p}^k \|\mu_{i,p}^k - \sum_{j=1}^{\mathcal{K}} \pi_{i,p}^j \mu_{i,p}^j\|_2^2 \quad (10)$$

$$\sigma_a^2 = \sum_{p=1}^{C_r} \sum_{k=1}^{\mathcal{K}} \pi_{i,p}^k \Sigma_{i,p}^k \quad (11)$$

where the mean, variance, and mixture weights for the p^{th} predicate class are estimated as follows:

$$\mu_i^k = f_\mu^k(\mathbf{z}_i), \Sigma_i^k = \sigma(f_\Sigma^k(\mathbf{z}_i)), \pi_i^k = \frac{e^{f_\pi^k(\mathbf{z}_i)}}{\sum_{k=1}^{\mathcal{K}} e^{f_\pi^k(\mathbf{z}_i)}} \quad (12)$$

where f_μ, f_Σ, f_π are the FFN projection functions and σ is the sigmoid non-linearity which ensures $\Sigma_{i,p}^k \geq 0$ for the p^{th} predicate class. During training, $\mathbf{z}_i = \hat{r}_{tem}^i$, the mixture of attenuated loss (\mathcal{L}_{MAL}) is given as:

$$\mathcal{L}_{MAL} = \frac{1}{N} \sum_{i=1}^N \sum_{p=1}^{C_r} \sum_{k=1}^{\mathcal{K}} \pi_{i,p}^k \frac{\mathcal{L}(\mu_{i,p}^k, y_{r_p}^i)}{\Sigma_{i,p}^k} \quad (13)$$

where $\mathcal{L}(\mu_{i,p}^k, y_{r_p}^i)$ is the sigmoidal cross entropy loss, $y_{r_p}^i$ is the ground-truth predicate class mapped to \mathbf{z}_i , $\mu_{i,p}^k$ is logit of label p in k^{th} mixture. For the corrupted input it is more likely to make a false prediction, hence $\Sigma_{i,p}^k$ will increase to reduce the overall loss function for such instance, which in turn prevents over-fitting to the corrupted instances making model more robust.

Uncertainty-aware Supervised Contrastive Learning: The MAL loss function classifies labels independently; this makes it difficult to capture correlations between co-occurring semantic labels. To address this limitation, we propose kernel-based multi-label contrastive loss, i.e., \mathcal{L}_{KMCL} . The objective of this loss function is to pull together the representations of predicates sharing at least one class with the anchor representation \hat{r}_{tem}^n while pushing apart negative samples that do not share any classes. Let us consider the positive set $\mathcal{A}(n) = \{m \in \{N \setminus n\} : \mathcal{Y}_r^n \cdot \mathcal{Y}_r^m \neq 0, \text{ where } \cdot \text{ is a dot product}\}$ contains samples that have at least one label in common with the anchor \hat{r}_{tem}^n , while $\mathcal{Y}_r(n, m) = \{y_{r_p} \in \mathcal{Y}_r : y_{r_p}^n = y_{r_p}^m = 1\}$ represents the indices of shared labels between \hat{r}_{tem}^n and \hat{r}_{tem}^m . The loss is

formulated as:

$$\mathcal{L}_{KMCL} = \frac{1}{N} \sum_{n=1}^N \frac{-1}{|\mathcal{A}(n)|} \sum_{m \in \mathcal{A}(n)} J(n, m) \sum_{y_{r_p} \in \mathcal{Y}_r(n, m)} \left(\log \frac{\exp(\rho_{y_{r_p}}^{n, m} / \tau)}{\sum_{i \in N \setminus n} \exp(\rho_{y_{r_p}}^{n, i} / \tau)} \right) \quad (14)$$

where kernel similarity is given as:

$$\rho_{y_{r_p}}^{n, i} = \left(\prod_{k=1}^{\mathcal{K}} \left(\frac{(\Sigma_{n,p}^k)^2 + (\Sigma_{i,p}^k)^2}{2(\Sigma_{n,p}^k)(\Sigma_{i,p}^k)} \right)^{-\frac{1}{2}} \right) \exp \left(-\frac{1}{4} \sum_{k=1}^{\mathcal{K}} \frac{(\mu_{n,p}^k - \mu_{i,p}^k)^2}{(\Sigma_{n,p}^k)^2 + (\Sigma_{i,p}^k)^2} \right) \quad (15)$$

EMA Teacher: During training, we adopt the EMA weight update [2, 20, 45, 47] for transformers in Section 3.3. Let's say ϕ_T, θ_T are the weights of transformers for teacher and student, respectively. The weight update is then given as:

$$\phi_{T,e} = \alpha * \phi_{T,e-1} + (1 - \alpha) * \theta_{T,e} \quad (16)$$

where e is the training epoch. The EMA teacher effectively an ensemble of student models at different training steps, which is a most widely used learning strategy in semi-supervised setting [10, 15, 41, 45]. With combined effect of all the student models the teacher model is an unbiased estimator of predicate embeddings, resulting in improved performance.

3.6. Training and Testing

Training: With flow based object predictor (Section 3.2) and correlation-aware predicate embeddings, the debiased predicate embeddings (Section 3.3, 3.4) is generated. The entire framework is trained end-to-end minimizing the loss equation:

$$\mathcal{L} = \mathcal{L}_o + \mathcal{L}_{MAL} + \mathcal{L}_{KMCL} - \lambda_1 \sigma_e + \lambda_2 \sigma_a \quad (17)$$

Testing: During testing we utilize the EMA teacher ϕ_T to generate the predicate embeddings \hat{r}_{tem}^i . These predicate embeddings are then passed to MLN which outputs the predicate confidence scores, $\hat{y}_{r_p}^i$. The predicate confidence scores from \mathcal{K} mixtures is given as:

$$\hat{y}_{r_p}^i = \sum_{k=1}^{\mathcal{K}} \pi_{i,p}^k \frac{\mu_{i,p}^k}{\Sigma_{i,p}^k} \quad (18)$$

4. Experiments

4.1. Dataset and Implementation

Dataset: Following previous works [6, 31], we also evaluated our method on the most widely used benchmark, Action Genome [16]. Action Genome is the largest benchmark

for video SGG; it is built on top of Charades[39]. It contains 476,229 bounding boxes for 35 object classes (without person) and 1,715,568 instances of 26 predicate classes annotated for 234,253 frames. For all experiments, we use the same training and test split following [6, 26, 31].

Metrics and Evaluation Setup: We evaluated the performance of FLOCODE with popular metrics, namely, recall@K (i.e., R@K) and mean-recall@K (i.e., mR@K), for $K = [10, 20, 50]$. R@K measures the ratio of correct instances among the top-K predicted instances with the highest confidence, but this is biased towards frequent predicate classes [43], whereas mR@K averages out the R@K over all relationships. Hence, mR@K is a more reliable metric for balanced evaluation across predicates [43].

Tasks: Following previous works [6, 16, 22, 46], we also evaluated our method on three different experimental tasks: 1) **Predicate Classification (PREDCLS)**: predict the predicate class of object pairs, given the ground-truth bounding boxes and labels of objects. 2) **Scene graph classification (SGCLS)**: predict both predicate labels and the category labels of objects given the bounding boxes of objects. 3) **Scene graph detection (SGDET)**: simultaneously detects objects appearing in the frame and the predicate labels of each object pair in a frame. Following, we also evaluated our method using two setups: a) **With Constraint** and b) **No Constraints**. Later one allows each object pair to have more than one predicates simultaneously while the former one restricts to only one predicate.

Implementation details: Following previous works [6, 16, 22, 31, 46], we adopted FasterRCNN [37] with ResNet-101 [13] backbone as the object detector. We train the object detector on the training set of Action Genome[16]; this results in 24.6 mAP at 0.5 IoU with CoCo metrics. For a fair comparison, we used this detector across all the baselines. Following previous works [6, 16, 22, 31, 46], per-class non-maximal suppression at 0.4 IoU (intersection over union) is applied to reduce region proposals provided by RPN. The parameters of the object detector (excluding the object classifier) are fixed during training when training scene graph generation models. For correlation-aware predicate embedding, it is required to match the object pairs across the frames. If there are multiple objects in the same category, to distinguish different pairs, we use IoU between the two objects across different images to match the subject-object pair. We calculated the IoU between the bounding box of the object in the previous frame and the object of the same category in the next frame. If the IoU is higher than 0.8, we consider them to be the same object. If there are multiple candidates, we choose the one with the highest IoU. We use an AdamW optimizer [29] with a batch size of 1 and an initial learning rate of $2e^{-5}$. The number of mixture components \mathcal{K} is set to 4 for SGCLS and 6 for PREDCLS and SGDET. The self-attention and cross-attention layers in our

framework have 8 heads with $d = 1536$ and dropout= 0.1. We set regularizer hyper-parameters as $\lambda_1 = 1, \lambda_2 = 1$. For debaised predicate embedding, we set the initial learning rate of $1e^{-5}$ and reduce it with patience to 3. For the EMA teacher update, we have used $\alpha = 0.999$. All experiments are carried out on a single NVIDIA RTX-3090.

4.2. Comparison with state-of-the-art

We compared our method FLOCODE with several state-of-the-art methods for dynamic SGG, namely, TEMPURA [31], STTran [6], TRACE [46], STTran-TPI [50], APT [26], and ISGG [21]. Additionally, we compared our method with ReLDN [58], which is a static method. Performance comparisons in terms of mR@K and R@K for $K = [10, 20, 50]$ are reported in Tables 1, 2, and 3. These tables contain comparisons with two experimental setups: a) **With Constraint** and b) **No Constraints**. With these experimental setups and tasks, i.e., *PREDCLS* + *SGCLS*, we presented results for these in terms of mR@K and R@K in Tables 2 and 3, respectively. Table 1 compares results for task i.e., *SGDET*, with the same metrics and under both experimental setups. Wherever available, we utilise the source code for the respective SOTA methods for mR@K and R@K values. For methods with no code, we take the values reported in [31]. From the tables, it has been observed that our method consistently outperforms other methods across all the tasks and for both experimental setups. Specifically, in comparison to the best baselines, we observe improvements of 4.1% on *SGDET*-mR@10, 3.4% on *SGCLS*-mR@10, and 1.9% on *PREDCLS*-mR@10 under the “**With Constraint**” setup. Under the “**No Constraints**” setup, we observe improvements even more significant, with 3.9% on *SGDET*-mR@10, 1.4% on *SGCLS*-mR@10, and 1.7% on *PREDCLS*-mR@10. This demonstrated the capability of FLOCODE in generating more unbiased SGG for videos incorporating dynamic fluctuations and long-tailed relations. We further verified this in Figure 3 for **With Constraint** and **No Constraints**. In these figures, we compared our method on HEAD, BODY, and TAIL classes with mR@10 values. We split the classes into HEAD, BODY, and TAIL with the same definition as mentioned in [31]. Clearly, FLOCODE improved the performance across all the classes, but the improvement for TAIL classes is more confirming the unbiased predictions. Per-class performance is shown in Fig. 4, comparing with other methods *STTran* and *TRACE* showing the improvement at class level. Additionally, our method outperforms in terms of R@K values, as shown in Table 3, showing improvements overall as compared to existing methods. This demonstrates that our method has better generalisation since it performs better on both mR@K (long tail performance) and R@K (overall). Qualitative visualisations are illustrated in Fig 2.

Method	With Constraint						No Constraint					
	mR@10	mR@20	mR@50	R@10	R@20	R@50	mR@10	mR@20	mR@50	R@10	R@20	R@50
RelDN	3.3	3.3	3.3	9.1	9.1	9.1	7.5	18.8	33.7	13.6	23.0	36.6
HCRD supervised	-	8.3	9.1	-	27.9	30.4	-	-	-	-	-	-
TRACE	8.2	8.2	8.2	13.9	14.5	14.5	22.8	31.3	41.8	26.5	35.6	45.3
ISGG	-	19.7	22.9	-	29.2	35.3	-	-	-	-	-	-
STTran	16.6	20.8	22.2	25.2	34.1	37.0	20.9	29.7	39.2	24.6	36.2	48.8
STTran-TPI	15.6	20.2	21.8	26.2	34.6	37.4	-	-	-	-	-	-
APT	-	-	-	26.3	36.1	38.3	-	-	-	25.7	37.9	50.1
TEMPURA	18.5	22.6	23.7	28.1	33.4	34.9	24.7	33.9	43.7	29.8	38.1	46.4
FloCoDe	22.6	24.2	27.9	31.5	38.4	42.4	28.6	35.4	47.2	32.6	43.9	51.6

Table 1. Comparative results for SGDET task, on AG[16] in terms of mean-Recall@K and Recall@K, best results are in bold.

Method	With Constraint						No Constraints					
	PredCLS			SGCLS			PredCLS			SGCLS		
	mR@10	mR@20	mR@50	mR@10	mR@20	mR@50	mR@10	mR@20	mR@50	mR@10	mR@20	mR@50
RelDN	6.2	6.2	6.2	3.4	3.4	3.4	31.2	63.1	75.5	18.6	36.9	42.6
TRACE	15.2	15.2	15.2	8.9	8.9	8.9	50.9	73.6	82.7	31.9	42.7	46.3
STTran	37.8	40.1	40.2	27.2	28.0	28.0	51.4	67.7	82.7	40.7	50.1	58.8
STTran-TPI	37.3	40.6	40.6	28.3	29.3	29.3	-	-	-	-	-	-
TEMPURA	42.9	46.3	46.3	34.0	35.2	35.2	61.5	85.1	98.0	48.3	61.1	66.4
FloCoDe	44.8	49.2	49.3	37.4	39.2	39.4	63.2	86.9	98.6	49.7	63.8	69.2

Table 2. Comparative results for PREDCLS and SGCLS task, on AG[16] in terms of mean-Recall@K, best results are in bold.

Method	With Constraint						No Constraints					
	PredCLS			SGCLS			PredCLS			SGCLS		
	R@10	R@20	R@50	R@10	R@20	R@50	R@10	R@20	R@50	R@10	R@20	R@50
RelDN	20.3	20.3	20.3	11.0	11.0	11.0	44.2	75.4	89.2	25.0	41.9	47.9
TRACE	27.5	27.5	27.5	14.8	14.8	14.8	72.6	91.6	96.4	37.1	46.7	50.5
STTran	68.6	71.8	71.8	46.4	47.5	47.5	77.9	94.2	99.1	54.0	63.7	66.4
STTran-TPI	69.7	72.6	72.6	47.2	48.3	48.3	-	-	-	-	-	-
APT	69.4	73.8	73.8	47.2	48.9	48.9	78.5	95.1	99.2	55.1	65.1	68.7
TEMPURA	68.8	71.5	71.5	47.2	48.3	48.3	80.4	94.2	99.4	56.3	64.7	67.9
FloCoDe	70.1	74.2	74.2	48.4	51.2	51.2	82.8	97.2	99.9	57.4	66.2	68.8

Table 3. Comparative results for PREDCLS and SGCLS task, on AG[16] in terms of Recall@K, best results are in bold.

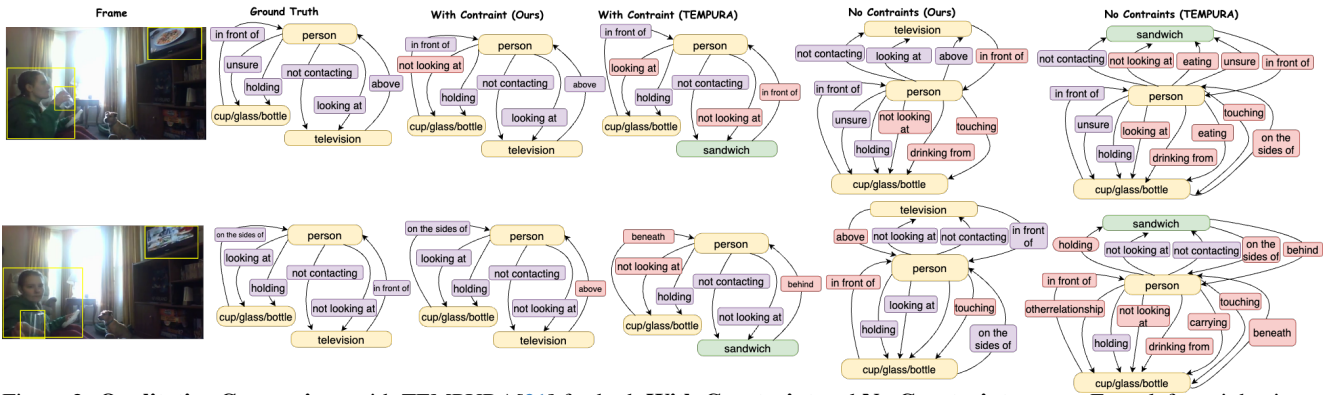


Figure 2. **Qualitative Comparison** with TEMPURA[31] for both **With Constraint** and **No Constraints** setup. From left to right: input video frames, ground truth graphs, graphs generated by FLOCoDe, graphs generated by TEMPURA[31]. Incorrect object and predicate predictions are shown in green and red, respectively.

Uncertainty-aware Contrastive Learning	Correlation-aware Debiasing	Flow-aware Temporal Consistency	Regularizer	EMA Teacher	With Constraint				No Constraints			
					SGCLS		SGDET		SGCLS		SGDET	
					mR@10	mR@20	mR@10	mR@20	mR@10	mR@20	mR@10	mR@20
-	-	-	-	-	27.2	28.0	16.5	20.8	40.7	50.1	20.9	29.7
✓	-	✓	✓	✓	34.1	33.8	19.6	22.1	46.9	61.1	26.6	32.7
-	✓	✓	✓	✓	33.6	34.3	19.4	21.8	46.2	60.6	25.8	32.5
✓	✓	-	✓	✓	32.2	33.4	18.1	19.8	45.9	59.1	21.8	31.6
✓	✓	✓	-	✓	35.8	36.6	21.2	22.7	48.3	61.4	27.5	34.4
✓	✓	✓	✓	-	36.7	38.8	22.1	23.8	49.2	62.9	28.3	35.2
✓	✓	✓	✓	✓	37.4	39.2	22.6	24.2	49.7	63.8	28.6	35.4

Table 4. **Ablation Studies:** Importance of *KMCL*, *Debiasing*, *TFoD*, *Regularizer* & *EMA Teacher* for SGCLS and SGDET.

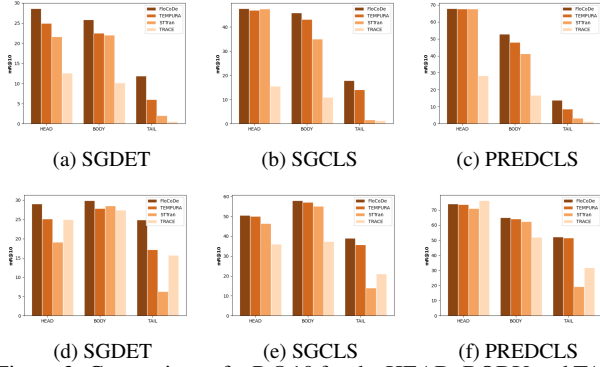


Figure 3. Comparison of mR@10 for the HEAD, BODY and TAIL classes for "with constraint"(top) and "no constraints"(bottom)

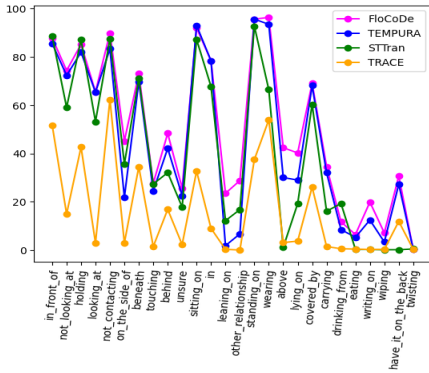


Figure 4. Comparative per class performance for PREDCLS task in R@10 for "with constraint" setup

Task \ \mathcal{K}	1	2	4	6	8
PREDCLS	39.8	41.2	43.4	44.8	44.2
SGCLS	30.2	35.5	37.4	36.2	35.8
SGDET	16.1	18.1	21.9	22.6	22.1

Table 5. Results (in mR@10) with varying number of mixtures \mathcal{K} for **With Constraint** setup

4.3. Ablation Studies

We have conducted extensive ablation studies on SGCLS and SGDET tasks. Specifically, we studied the impact of

KMCL (uncertainty-aware contrastive learning), *Debiasing* (correlation-aware debiasing), *TFoD* (flow-aware temporal consistency), *Regularizer* (aleatoric and epistemic regularizer), and *EMA Teacher*. When all these components have been removed, the FLOCODE boils down to the baseline STTran[6], where the object proposals and predicate embeddings are fed to the FFN layers before finally predicting the predicate class using a classification layer. The results for these ablation studies are presented in Table 4. **Uncertainty Attenuation and Debiasing:** We first discuss the impact of uncertainty-aware contrastive learning and correlation-aware debiasing. For the first case, we remove the loss \mathcal{L}_{KMCL} to study the improvement on top of the loss based on MLN. With MLN mixtures, a similar improvement is already demonstrated in [31]. In the second case, we remove the correlation-aware debiasing during training and train end-to-end without any debiasing. The results for both of these are present in Table 4 rows 1 and 2. Clearly, comparing the resulting models with FLOCODE shows the significant improvement in mR@10 values, showing the value addition from each of them in generating an unbiased SGG. This also shows that both can address the noise associated with TAIL classes, while contrastive learning deals with annotation noise-debiasing focus to generate unbiased predicate embeddings. **Temporally Consistent Object Detection:** The effect of flow-aware detection of temporally consistent objects is shown in row 3 of Table 4. Comparing the performance with FLOCODE, we can see that without *TFoD* results in a significant drop in performance. This highlights the fact that incorrect object detection is the major bottleneck for any SGG method. For *PREDCLS* task, it takes only the ground-truth boxes and labels, and hence the mR@k and R@K values are much higher as compared to other tasks. **Uncertainty Regularizer and EMA Teacher:** Comparing the ablation of these two components from rows 4 and 5, respectively, confirms the importance of regularizers in further reducing the noise associated with the TAIL classes. For EMA teachers, it produces more balanced predicate embeddings, hence providing improvement by just predicting the unbiased embeddings corresponding to their class. **Number of Mixtures \mathcal{K} :** The performance of FLOCODE with varying numbers of mixtures in MLN is shown in Ta-

ble 5. Number of mixtures b/w 4 to 6 is optimal.

5. Conclusion

We demonstrated the correlation debiasing (label correlation and debiased predicate embedding) and resulting performance of FLOCODE with these debiasing mechanism prove the fact that dynamic SGG requires more focus on long-tailed classification rather than complex architecture for temporal sequence processing.

References

- [1] Stanislaw Antol, Aishwarya Agrawal, Jiasen Lu, Margaret Mitchell, Dhruv Batra, C Lawrence Zitnick, and Devi Parikh. Vqa: Visual question answering. In *Proceedings of the IEEE international conference on computer vision*, pages 2425–2433, 2015. 1
- [2] Nikita Araslanov and Stefan Roth. Self-supervised augmentation consistency for adapting semantic segmentation. In *Proceedings of the IEEE/CVF Conference on Computer Vision and Pattern Recognition*, pages 15384–15394, 2021. 5
- [3] Anurag Arnab, Mostafa Dehghani, Georg Heigold, Chen Sun, Mario Lučić, and Cordelia Schmid. Vivit: A video vision transformer. In *Proceedings of the IEEE/CVF international conference on computer vision*, pages 6836–6846, 2021. 1, 2
- [4] Nicolas Carion, Francisco Massa, Gabriel Synnaeve, Nicolas Usunier, Alexander Kirillov, and Sergey Zagoruyko. End-to-end object detection with transformers. In *European conference on computer vision*, pages 213–229. Springer, 2020. 1
- [5] Tianshui Chen, Weihao Yu, Riquan Chen, and Liang Lin. Knowledge-embedded routing network for scene graph generation. In *Proceedings of the IEEE/CVF Conference on Computer Vision and Pattern Recognition*, pages 6163–6171, 2019. 1
- [6] Yuren Cong, Wentong Liao, Hanno Ackermann, Bodo Rosenhahn, and Michael Ying Yang. Spatial-temporal transformer for dynamic scene graph generation. In *Proceedings of the IEEE/CVF international conference on computer vision*, pages 16372–16382, 2021. 1, 2, 3, 5, 6, 8
- [7] Alakh Desai, Tz-Ying Wu, Subarna Tripathi, and Nuno Vasconcelos. Learning of visual relations: The devil is in the tails. In *Proceedings of the IEEE/CVF International Conference on Computer Vision*, pages 15404–15413, 2021. 1
- [8] Jianfeng Dong, Xirong Li, Chaoxi Xu, Xun Yang, Gang Yang, Xun Wang, and Meng Wang. Dual encoding for video retrieval by text. *IEEE Transactions on Pattern Analysis and Machine Intelligence*, 44(8):4065–4080, 2021. 1
- [9] Alexey Dosovitskiy, Philipp Fischer, Eddy Ilg, Philip Hausser, Caner Hazirbas, Vladimir Golkov, Patrick Van Der Smagt, Daniel Cremers, and Thomas Brox. FlowNet: Learning optical flow with convolutional networks. In *Proceedings of the IEEE international conference on computer vision*, pages 2758–2766, 2015. 3
- [10] Geoff French, Samuli Laine, Timo Aila, Michal Mackiewicz, and Graham Finlayson. Semi-supervised semantic segmentation needs strong, varied perturbations. *arXiv preprint arXiv:1906.01916*, 2019. 5
- [11] Raghav Goyal¹² and Leonid Sigal¹²³. A simple baseline for weakly-supervised human-centric relation detection. 2021. 1
- [12] Kai Han, Yunhe Wang, Hanting Chen, Xinghao Chen, Jianyuan Guo, Zhenhua Liu, Yehui Tang, An Xiao, Chun-jing Xu, Yixing Xu, et al. A survey on vision transformer. *IEEE transactions on pattern analysis and machine intelligence*, 45(1):87–110, 2022. 1
- [13] Kaiming He, Xiangyu Zhang, Shaoqing Ren, and Jian Sun. Deep residual learning for image recognition. In *Proceedings of the IEEE conference on computer vision and pattern recognition*, pages 770–778, 2016. 2, 6
- [14] Kaiming He, Georgia Gkioxari, Piotr Dollár, and Ross Girshick. Mask r-cnn. In *Proceedings of the IEEE international conference on computer vision*, pages 2961–2969, 2017. 2, 4
- [15] Lukas Hoyer, Dengxin Dai, Yuhua Chen, Adrian Koring, Suman Saha, and Luc Van Gool. Three ways to improve semantic segmentation with self-supervised depth estimation. In *Proceedings of the IEEE/CVF Conference on Computer Vision and Pattern Recognition*, pages 11130–11140, 2021. 5
- [16] Jingwei Ji, Ranjay Krishna, Li Fei-Fei, and Juan Carlos Niebles. Action genome: Actions as compositions of spatio-temporal scene graphs. In *Proceedings of the IEEE/CVF Conference on Computer Vision and Pattern Recognition*, pages 10236–10247, 2020. 2, 5, 6, 7
- [17] Jingwei Ji, Rishi Desai, and Juan Carlos Niebles. Detecting human-object relationships in videos. In *Proceedings of the IEEE/CVF International Conference on Computer Vision*, pages 8106–8116, 2021. 1, 3
- [18] Chen Ju, Tengda Han, Kunhao Zheng, Ya Zhang, and Weidi Xie. Prompting visual-language models for efficient video understanding. In *European Conference on Computer Vision*, pages 105–124. Springer, 2022. 1
- [19] Alex Kendall and Yarin Gal. What uncertainties do we need in bayesian deep learning for computer vision? *Advances in neural information processing systems*, 30, 2017. 1
- [20] Anant Khandelwal. Segda: Maximum separable segment mask with pseudo labels for domain adaptive semantic segmentation. In *Proceedings of the IEEE/CVF International Conference on Computer Vision*, pages 2158–2168, 2023. 5
- [21] Siddhesh Khandelwal and Leonid Sigal. Iterative scene graph generation. *Advances in Neural Information Processing Systems*, 35:24295–24308, 2022. 6
- [22] Ranjay Krishna, Yuke Zhu, Oliver Groth, Justin Johnson, Kenji Hata, Joshua Kravitz, Stephanie Chen, Yannis Kalantidis, Li-Jia Li, David A Shamma, et al. Visual genome: Connecting language and vision using crowdsourced dense image annotations. *International journal of computer vision*, 123:32–73, 2017. 1, 2, 6
- [23] Rongjie Li, Songyang Zhang, and Xuming He. Sgtr: End-to-end scene graph generation with transformer. In *proceedings of the IEEE/CVF conference on computer vision and pattern recognition*, pages 19486–19496, 2022.
- [24] Yikang Li, Wanli Ouyang, Bolei Zhou, Kun Wang, and Xiaogang Wang. Scene graph generation from objects, phrases

- and region captions. In *Proceedings of the IEEE international conference on computer vision*, pages 1261–1270, 2017. [1](#), [2](#)
- [25] Yicong Li, Xun Yang, Xindi Shang, and Tat-Seng Chua. Interventional video relation detection. In *Proceedings of the 29th ACM International Conference on Multimedia*, pages 4091–4099, 2021. [1](#)
- [26] Yiming Li, Xiaoshan Yang, and Changsheng Xu. Dynamic scene graph generation via anticipatory pre-training. In *Proceedings of the IEEE/CVF Conference on Computer Vision and Pattern Recognition*, pages 13874–13883, 2022. [1](#), [2](#), [3](#), [6](#)
- [27] Xin Lin, Changxing Ding, Jinquan Zeng, and Dacheng Tao. Gps-net: Graph property sensing network for scene graph generation. In *Proceedings of the IEEE/CVF Conference on Computer Vision and Pattern Recognition*, pages 3746–3753, 2020. [1](#), [2](#)
- [28] Chenchen Liu, Yang Jin, Kehan Xu, Guoqiang Gong, and Yadong Mu. Beyond short-term snippet: Video relation detection with spatio-temporal global context. In *Proceedings of the IEEE/CVF conference on computer vision and pattern recognition*, pages 10840–10849, 2020. [1](#), [2](#)
- [29] Ilya Loshchilov and Frank Hutter. Decoupled weight decay regularization. *arXiv preprint arXiv:1711.05101*, 2017. [6](#)
- [30] Cewu Lu, Ranjay Krishna, Michael Bernstein, and Li Fei-Fei. Visual relationship detection with language priors. In *Computer Vision–ECCV 2016: 14th European Conference, Amsterdam, The Netherlands, October 11–14, 2016, Proceedings, Part I 14*, pages 852–869. Springer, 2016. [1](#), [2](#)
- [31] Sayak Nag, Kyle Min, Subarna Tripathi, and Amit K Roy-Chowdhury. Unbiased scene graph generation in videos. In *Proceedings of the IEEE/CVF Conference on Computer Vision and Pattern Recognition*, pages 22803–22813, 2023. [1](#), [2](#), [4](#), [5](#), [6](#), [7](#), [8](#)
- [32] Megha Nawhal and Greg Mori. Activity graph transformer for temporal action localization. *arXiv preprint arXiv:2101.08540*, 2021. [1](#), [2](#)
- [33] Vardan Papyan, XY Han, and David L Donoho. Prevalence of neural collapse during the terminal phase of deep learning training. *Proceedings of the National Academy of Sciences*, 117(40):24652–24663, 2020. [3](#)
- [34] Jeongeun Park, Seungyou Shin, Sangheum Hwang, and Sungjoon Choi. Elucidating robust learning with uncertainty-aware corruption pattern estimation. *Pattern Recognition*, 138:109387, 2023. [1](#)
- [35] Tao Pu, Tianshui Chen, Hefeng Wu, Yongyi Lu, and Liang Lin. Spatial-temporal knowledge-embedded transformer for video scene graph generation. *arXiv preprint arXiv:2309.13237*, 2023. [1](#)
- [36] Xufeng Qian, Yueting Zhuang, Yimeng Li, Shaoning Xiao, Shiliang Pu, and Jun Xiao. Video relation detection with spatio-temporal graph. In *Proceedings of the 27th ACM international conference on multimedia*, pages 84–93, 2019. [1](#), [2](#)
- [37] Shaoqing Ren, Kaiming He, Ross Girshick, and Jian Sun. Faster r-cnn: Towards real-time object detection with region proposal networks. *Advances in neural information processing systems*, 28, 2015. [2](#), [6](#)
- [38] Ahmad Sajedi, Samir Khaki, Konstantinos N Plataniotis, and Mahdi S Hosseini. End-to-end supervised multilabel contrastive learning. *arXiv preprint arXiv:2307.03967*, 2023. [1](#)
- [39] Gunnar A Sigurdsson, Gül Varol, Xiaolong Wang, Ali Farhadi, Ivan Laptev, and Abhinav Gupta. Hollywood in homes: Crowdsourcing data collection for activity understanding. In *Computer Vision–ECCV 2016: 14th European Conference, Amsterdam, The Netherlands, October 11–14, 2016, Proceedings, Part I 14*, pages 510–526. Springer, 2016. [6](#)
- [40] Cees GM Snoek, Marcel Worring, et al. Concept-based video retrieval. *Foundations and Trends® in Information Retrieval*, 2(4):215–322, 2009. [1](#)
- [41] Kihyuk Sohn, David Berthelot, Nicholas Carlini, Zizhao Zhang, Han Zhang, Colin A Raffel, Ekin Dogus Cubuk, Alexey Kurakin, and Chun-Liang Li. Fixmatch: Simplifying semi-supervised learning with consistency and confidence. *Advances in neural information processing systems*, 33:596–608, 2020. [5](#)
- [42] Chen Sun, Austin Myers, Carl Vondrick, Kevin Murphy, and Cordelia Schmid. Videobert: A joint model for video and language representation learning. In *Proceedings of the IEEE/CVF international conference on computer vision*, pages 7464–7473, 2019. [1](#), [2](#)
- [43] Kaihua Tang, Hanwang Zhang, Baoyuan Wu, Wenhan Luo, and Wei Liu. Learning to compose dynamic tree structures for visual contexts. In *Proceedings of the IEEE/CVF conference on computer vision and pattern recognition*, pages 6619–6628, 2019. [1](#), [2](#), [6](#)
- [44] Makarand Tapaswi, Yukun Zhu, Rainer Stiefelhausen, Antonio Torralba, Raquel Urtasun, and Sanja Fidler. Movieqa: Understanding stories in movies through question-answering. In *Proceedings of the IEEE conference on computer vision and pattern recognition*, pages 4631–4640, 2016. [1](#)
- [45] Antti Tarvainen and Harri Valpola. Mean teachers are better role models: Weight-averaged consistency targets improve semi-supervised deep learning results. *Advances in neural information processing systems*, 30, 2017. [5](#)
- [46] Yao Teng, Limin Wang, Zhifeng Li, and Gangshan Wu. Target adaptive context aggregation for video scene graph generation. In *Proceedings of the IEEE/CVF International Conference on Computer Vision*, pages 13688–13697, 2021. [1](#), [2](#), [6](#)
- [47] Wilhelm Truhner, Viktor Olsson, Juliano Pinto, and Lennart Svensson. Dacs: Domain adaptation via cross-domain mixed sampling. In *Proceedings of the IEEE/CVF Winter Conference on Applications of Computer Vision*, pages 1379–1389, 2021. [5](#)
- [48] Yao-Hung Hubert Tsai, Santosh Divvala, Louis-Philippe Morency, Ruslan Salakhutdinov, and Ali Farhadi. Video relationship reasoning using gated spatio-temporal energy graph. In *Proceedings of the IEEE/CVF Conference on Computer Vision and Pattern Recognition*, pages 10424–10433, 2019. [2](#)
- [49] Ashish Vaswani, Noam Shazeer, Niki Parmar, Jakob Uszkoreit, Llion Jones, Aidan N Gomez, Łukasz Kaiser, and Illia

- Polosukhin. Attention is all you need. *Advances in neural information processing systems*, 30, 2017. 1, 2, 3
- [50] Shuang Wang, Lianli Gao, Xinyu Lyu, Yuyu Guo, Pengpeng Zeng, and Jingkuan Song. Dynamic scene graph generation via temporal prior inference. In *Proceedings of the 30th ACM International Conference on Multimedia*, pages 5793–5801, 2022. 2, 3, 6
- [51] Yinwei Wei, Xiang Wang, Weili Guan, Liqiang Nie, Zhouchen Lin, and Baoquan Chen. Neural multimodal cooperative learning toward micro-video understanding. *IEEE Transactions on Image Processing*, 29:1–14, 2019. 1
- [52] Junbin Xiao, Xindi Shang, Angela Yao, and Tat-Seng Chua. Next-qa: Next phase of question-answering to explaining temporal actions. In *Proceedings of the IEEE/CVF conference on computer vision and pattern recognition*, pages 9777–9786, 2021. 1
- [53] Kelvin Xu, Jimmy Ba, Ryan Kiros, Kyunghyun Cho, Aaron Courville, Ruslan Salakhudinov, Rich Zemel, and Yoshua Bengio. Show, attend and tell: Neural image caption generation with visual attention. In *International conference on machine learning*, pages 2048–2057. PMLR, 2015. 1
- [54] Li Xu, Haoxuan Qu, Jason Kuen, Jiuxiang Gu, and Jun Liu. Meta spatio-temporal debiasing for video scene graph generation. In *European Conference on Computer Vision*, pages 374–390. Springer, 2022. 1
- [55] Yibo Yang, Haobo Yuan, Xiangtai Li, Zhouchen Lin, Philip Torr, and Dacheng Tao. Neural collapse inspired feature-classifier alignment for few-shot class incremental learning. *arXiv preprint arXiv:2302.03004*, 2023. 3
- [56] Sai Harsha Yelleni, Kumari Deepshikha, PK Srijith, and C Krishna Mohan. Monte carlo dropblock for modelling uncertainty in object detection. *Pattern Recognition*, page 110003, 2023. 1
- [57] Rowan Zellers, Mark Yatskar, Sam Thomson, and Yejin Choi. Neural motifs: Scene graph parsing with global context. In *Proceedings of the IEEE conference on computer vision and pattern recognition*, pages 5831–5840, 2018. 1, 2, 4
- [58] Ji Zhang, Kevin J Shih, Ahmed Elgammal, Andrew Tao, and Bryan Catanzaro. Graphical contrastive losses for scene graph parsing. In *Proceedings of the IEEE/CVF Conference on Computer Vision and Pattern Recognition*, pages 11535–11543, 2019. 1, 2, 6
- [59] Sipeng Zheng, Shizhe Chen, and Qin Jin. Vrdformer: End-to-end video visual relation detection with transformers. In *Proceedings of the IEEE/CVF Conference on Computer Vision and Pattern Recognition*, pages 18836–18846, 2022. 2
- [60] Xizhou Zhu, Yujie Wang, Jifeng Dai, Lu Yuan, and Yichen Wei. Flow-guided feature aggregation for video object detection. In *Proceedings of the IEEE international conference on computer vision*, pages 408–417, 2017. 3
- [61] Xizhou Zhu, Yuwen Xiong, Jifeng Dai, Lu Yuan, and Yichen Wei. Deep feature flow for video recognition. In *Proceedings of the IEEE conference on computer vision and pattern recognition*, pages 2349–2358, 2017. 3